IMPROVEMENT OF TRADITIONAL AND HYBRID INTERPOLATION TECHNIQUES USING SUPPORT VECTOR MACHINE FOR LAND SURFACE TEMPERATURE ANALYSIS IN URBAN AREAS

***Titipong PHOOPHATHONG* [1,4], *Teerawong LAOSUWAN* [1,4*], *Satith SANGPRADID* [2*], *Yannawut UTTARUK* [3], *Thinnakon ANGKAHAD* [1,4]**

DOI: 10.21163/GT_2025.201.21

ABSTRACT

Interpolation techniques are highly effective numerical methods for achieving comprehensive spatial data coverage without the need to measure data at every location within the study area. Traditional interpolation methods, such as Inverse Distance Weighted (IDW) and Kriging, are numerical computations that rely on mathematical models without considering environmental influences on the spatial factors being interpolated. On the other hand, Support Vector Machines (SVM) are machine learning algorithms designed to enhance the accuracy of numerical computations. This research aims to improve and compare traditional interpolation techniques, specifically IDW, Ordinary Kriging (OK), and OK + SVM. The latter technique combines the OK interpolation concept with SVM learning to classify land cover and weight the interpolation of spatial data related to Land Surface Temperature (LST) in urban areas. The study revealed that the IDW technique produced values of T_{max} and T_{min} that were the closest to the actual measured values, followed by OK + SVM and OK, respectively. Furthermore, when assessing the interpolated data from 1,650 points extracted from LST using each technique against statistical tests such as MAE, MSE, and RMSE, it was found that OK + SVM provided better results than IDW and OK. Therefore, OK + SVM enhances interpolation accuracy by incorporating land cover classification, outperforming IDW and OK in LST estimation.

***Key-words**: Mathematical Method; Support Vector Machines; Inverse Distance Weighted; Ordinary Kriging; Land Surface Temperature; Geostatistic; Non-geostatistic; Digital Image Processing.*

1. INTRODUCTION

Heat is a fundamental physical factor that affects the survival of all living organisms on Earth, as living organisms must maintain an appropriate thermal balance to survive (Prohmdirek et al, 2020; Nord & Giroud, 2020;). If organisms receive excessive heat from the environment, or conversely, if they lose too much heat to the environment, they may not be able to survive in those environments (Dahlke et al, 2020). Therefore, the amount of heat is essential for the survival of various life forms on Earth (Bennett et al, 2021). Generally, the level of heat is indicated or defined by the term "temperature". As such, temperature levels are used as a measure of heat in various systems, including environmental heat (Thompson et al, 2020).

[1]*Department of Physics, Faculty of Science, Mahasarakham University, Maha Sarakham 44150; 64010262003@msu.ac.th; teerawong@msu.ac.th; thinnakon.ang@gmail.com*
[2]*Department of Geoinformatics, Faculty of Informatics, Mahasarakham University, Maha Sarakham 44150, Thailand; satith.s@msu.ac.th*
[3]*Department of Biology, Faculty of Science, Mahasarakham University, Maha Sarakham 44150, Thailand; yannawut.u@msu.ac.th*
[4]*Space Technology and Geo-Informatics Research Unit, Faculty of Science, Mahasarakham University, Thailand 44150*
**Corresponding author*

The study and measurement of environmental heat are often explained by the average temperature of each area, which represents the temperature at various points within the study area (Huang et al, 2019). However, average temperature may be too broad a parameter for studying and measuring heat at every specific point within an area (Duan et al, 2019). This is because each area has variations in thermal energy depending on the environment and the specific conditions of the surface at each location (Venter et al, 2020). Therefore, to obtain heat data for every point within an area for more detailed spatial temperature studies, a parameter known as Land Surface Temperature (LST) has been studied.

LST is one of the widely studied spatial parameters because it reflects the temperature and weather conditions of the area. Hence, LST has been extensively researched (Phan & Kappas, 2018; Cristobal et al, 2018; Shahfahad et al, 2020; Cilek & Cilek, 2021; Auntarin et al, 2021; Kovács & Haidu, 2022). Assessing and managing LST is crucial for the survival of living organisms (Xiao et al, 2018). Estimating LST combined with interpolation processes is one of the methods that allows for accurate access to LST parameters (Guha & Govil, 2021; Palafox-Juárez et al, 2021; Binarti & Santoso, 2023). Interpolation is a mathematical method employed to approximate the values of unknown data points situated between established, known data points. This technique serves to bridge gaps in the data. Technical traders utilize interpolation to gain insights into historical price movements, even in the absence of complete information (Vedantu, 2024; Magyari-Sáska et al, 2025). Although remote sensing technology has advanced and can facilitate the calculation and estimation of LST parameters, this method is still an approximation based on the blackbody radiation principle measured by various satellite sensors (Pade & Mountrakis, 2018). This method also has limitations related to cloud cover and sky clarity (Li et al, 2023; Militino et al, 2019; Chen et al, 2020). Therefore, discrete ground temperature measurements combined with interpolation processes remain a popular method for studying LST parameters (Kartal & Sekertekin, 2022; khosravi & Balyani, 2019; Li et al, 2020). However, although interpolation methods are widely used for studying LST parameters, the number of measurement stations or sensors available to measure these parameters is limited. This limitation results in a smaller dataset for interpolation calculations, which in turn reduces the efficiency of the interpolation process (Giustini et al, 2019). Therefore, improving interpolation techniques is a potential approach for further studying and enhancing the acquisition of LST parameters (Shtiliyanova et al, 2017; Rosillon et al, 2024; Zhang & Du, 2019; Li et al, 2020).

The selection of models and interpolation calculations today is generally based on the spatial data distribution obtained, combined with various statistical parameters for decision making (Sanguesa et al, 2023; Fuhg et al, 2021). For instance, Ordinary Kriging interpolation requires variogram modeling of data distribution using various functions to create a variogram graph for model selection (Krivoruchho & Gribov, 2019). However, solely considering the statistical distribution of the data to be interpolated may not be sufficient to obtain accurate interpolated data (Moustapha et al, 2018). This is because each type of spatial data is influenced by various environmental factors, such as LST, which is directly influenced by land cover as a primary environmental factor (Karakus, 2019). To achieve complete and accurate interpolation of spatial data, particularly when the data involves multiple variables, only a few studies have explored the combined influences of environmental factors on spatial data interpolation (Du et al, 2020). Spatial data plays a crucial role in planning, risk assessment, and decision-making in environmental management (Granville et al, 2023) since it can represent different statuses at every location within the study area and can be analyzed and assessed for potential scenarios across various times and locations (Cai et al, 2019). However, obtaining such data is not feasible from every location directly due to limitations in manpower, equipment, budget, and difficult geographical access. As a result, the study and generation of spatial data often employ spatial interpolation processes in combination with geostatistical methods (Fouedjio & Klump, 2019).

The generation of spatial data from discrete measurements at various points within an area has been studied and developed for various research topics (Hu et al, 2019; Sekulic et al; 2020; Fung et al, 2022; Subedi et al, 2019), including spatial variable studies and mathematical model development for interpolation calculations. In this research, the spatial interpolation process is studied and compared, utilizing both traditional interpolation models (Inverse Distance Weighting : IDW), Ordinary Kriging (OK) and a new method. The new spatial interpolation model developed combines the Kriging interpolation concept with machine learning, specifically Support Vector Machines (SVM), to learn the environmental factors that influence the spatial variable known as LST. The objective of this study is to improve and compare the interpolation processes for the spatial variable LST using traditional interpolation methods from the non-geostatistics group using IDW, the geostatistics group using OK, and a new interpolation method that combines the Kriging interpolation concept with SVM machine learning to learn the environmental factors affecting the spatial variable LST. These factors involve learning the land cover that influences LST through SVM classification, implemented via the ArcGIS software.

2. MATERIALS AND METHODS

2.1. Study Area

The study area is Talat Sub-district, Mueang Maha Sarakham District, Maha Sarakham Province, Thailand (**Fig. 1**). Mueang Maha Sarakham District is situated in the central part of the province, leaning towards the eastern side. It covers an area of approximately 556.70 square kilometers. The district shares its borders with neighboring administrative areas as follows:

To the north, it borders the sub-districts of Tha Khon Yang and Makha in the Kantharawichai District of Maha Sarakham Province, as well as the sub-district of Kut Khong Chai in the Khong Chai District of Kalasin Province. To the east, it is adjacent to the sub-districts of Wang Saeng in the Kaedam District and Si Kaew and Muang Lat in the Mueang Roi Et District of Roi Et Province.

To the south, it shares boundaries with the sub-districts of Suea Koke and Ngu Ba in the Wapi Pathum District of Maha Sarakham Province. To the west, it borders the sub-districts of Kaeng Ka in the Kosum Phisai District and Bo Yai in the Borabue District of Maha Sarakham Province.

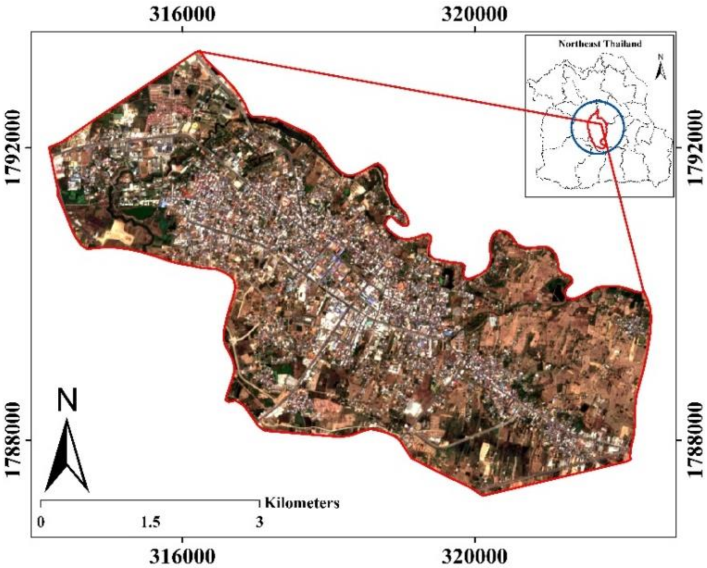

Fig. 1. Maps of Talat Sub-district, Mueang Maha Sarakham District, Maha Sarakham Province, Thailand.

The general topography of the area is a high plain with sandy or loamy soils. The average elevation ranges from 130 to 230 meters above mean sea level. The average temperature ranges from 27.91°C to 39.3°C, with a minimum temperature of 15.0°C. The area experiences three distinct seasons: the hot season from February to June, the rainy season from June to November, and the cold season from November to February. The average annual rainfall ranges from 1,000 to 1,200 millimeters. Most of Talat Sub-district is covered by residential buildings and various constructions, as it serves as the economic and commercial center of Maha Sarakham Province.

2.2. Methodology

To maintain conciseness in the presentation of this research, the operational method is illustrated in **Fig. 2**, with each aspect of the operation being detailed individually in the subsequent items.

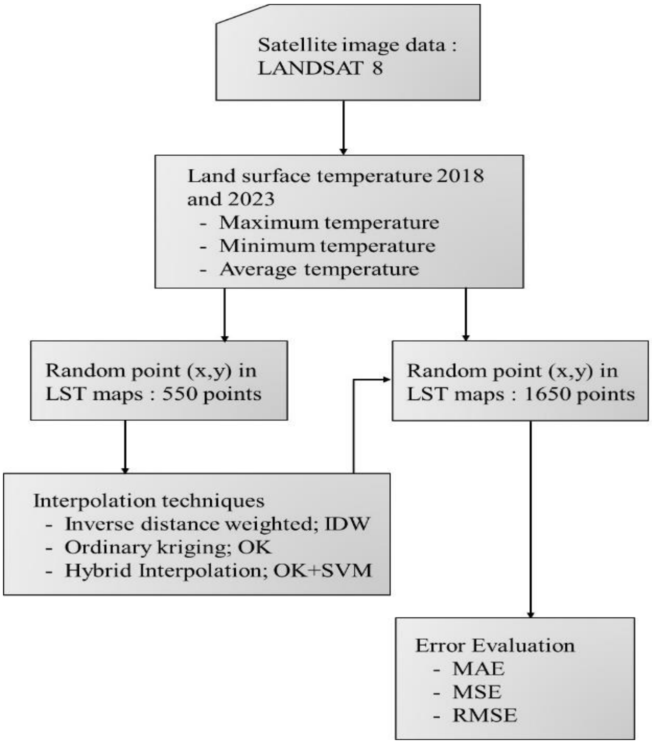

Fig. 2. The operational method.

2.2.1. Land Surface Temperature Analysis

Data from the LANDSAT-8 OLI/TIRS satellite, recorded in December of 2018 and 2023, were used to analyze Land Surface Temperature (LST) for this study. The LANDSAT-8 OLI/TIRS sensor features nine bands in the Operational Land Imager (OLI) range and two bands in the Thermal Infrared Sensor (TIRS) range, namely band 10 and band 11. The TIRS sensor was developed using new quantum physics technology to detect thermal radiation. TIRS detects the long wavelengths of light emitted from the Earth, whose intensity depends on LST. These wavelengths, called thermal infrared, are beyond the human visible spectrum. The specifications of the TIRS sensor are shown in **Table 1**.

Table 1.

The specifications of the TIRS sensor.

Landsat Band	Thernmal Band	Lower Band Edge (μm)	Upper Band Edge (μm)	Center Wavelength (μm)	Maximum Allowed Radiance Error Watts/(m^2/*srad*μm)
10	1	10.6	11.2	10.9	0.059 (0.4 K at 300 K)
11	2	11.5	12.5	12	0.049 (0.4 K at 300 K)

The data from TIRS (band 10), expressed in digital numbers (DN), was transformed into top-of-atmosphere (TOA) spectral radiance by utilizing the radiance rescaling factors detailed in the metadata file, as indicated in Equation 1 (Singh et al, 2022). Furthermore, the TIRS (band 10) data can be converted from spectral radiance to top-of-atmosphere brightness temperature by applying the thermal constants found in the MTL file, as outlined in Equation 2 (Rashid et al, 2022; Guha et al, 2020).

$$L_\lambda = M_L.Q_{cal} + A_L \tag{1}$$

where:
L_λ= TOA spectral radiance (Watts/(m2 *srad*μm))
M_L= Band-specific multiplicative rescaling factor from the metadata
A_L= Band-specific additive rescaling factor from the metadata
Q_{cal}= Quantized and calibrated standard product pixel values (DN)

$$BT = \frac{K_2}{In[\left(\frac{K_1}{L_\lambda}\right)+1]} - 273.15 \tag{2}$$

where:
BT = Top of atmosphere brightness temperature (K)
L_λ= TOA spectral radiance (Watts/(m^2 *srad*μm))
K_1, K_2= Band-specific thermal conversion constant from the metadata

2.2.2. Spatial Interpolation Analysis

Interpolation for the spatial interpolation process, whether using geostatistic or non-geostatistic methods, is widely used to address the spatial discontinuity of known data points. However, regardless of the interpolation technique employed, the concept of spatial interpolation is fundamentally based on Equation 3 (Yang et al, 2020). This describes the calculation and estimation of* unknown data points in an area based on known data points in that area using the weighted variable λ_i.When i represents the iteration of the number of known data points in the area. The weighted variable reflects the influence of neighboring known data and ensures that the interpolated data is appropriately weighted using various techniques and methods. From Equation 3, it can be observed that the interpolated data $Z(x_0)$ is derived from the summation of known data points in the area, each multiplied by the corresponding weighted variable at each location $Z(x_i)$ in the region.

$$Z(x_0) = \sum_{i=1}^{N} \lambda_i Z(x_i) \tag{3}$$

From Equation 3, it can be observed that the data obtained from the process of inserting the value $Z(x_0)$ results from the sum of known values in the area at position $Z(x_i)$, multiplied by the weighting variable at each position within that region.

2.2.3. Inverse Distance Weighting (IDW) Analysis

IDW is one of the most straightforward and basic spatial interpolation methods. Although it is not a geostatistical interpolation method, its basic concept involves calculating and estimating unknown data points from known data points. The closer the unknown point is to a known data point, the more influence that known data point will have on the interpolation result. Thus, this method considers the distance between the unknown and known data points as a key factor in interpolation, expressed in the weighted variable in Equation 4 (Singh & Verma; 2019). The final equation for the IDW interpolation process is shown in Equation 5 (Li, 2021).

$$\lambda_i = \frac{d_{ij}^{-p}}{\sum_{i=1}^{n} d_{ij}^{-p}} \tag{4}$$

where:
d_{ij} = The distance between the known value at position i and the value to be inserted at position j.
p = The total number of predictions for each validation case

Through this method, the net equation of the interpolation process using the IDW technique can be represented as shown in Equation 5.

$$Z_j = \frac{\sum_{i=1}^{N} z_{ij} d_{ij}^{-n}}{\sum_{i=1}^{N} d_{ij}^{-n}} \tag{5}$$

2.2.4. Ordinary Kriging (OK) Analysis

OK is one of the most basic methods for the Kriging process and is a geostatistical interpolation method. However, it still adheres to the general interpolation equation concept. This method analyzes data using a statistical model that examines the variance between two points, as shown in Equation 6 (Gai et al, 2019). The equation in Equation 6 serves as the basic calculation for Semi variance, which is further developed into a Variogram model, as shown in Equation 7 (Khan et al, 2023). The Variogram model is created to fit the curve according to the statistical distribution of the data, with examples of models including Spherical, Exponential, Linear, and Gaussian.

$$\gamma(X_i, X_0) = \gamma(h) = \frac{1}{2} var[(Z(X_i) - Z(X_0))] \tag{6}$$

$$\hat{\gamma}(h) = \frac{1}{2n} \sum_{i=1}^{n} (Z(X_i) - Z(X_i + h))^2 \tag{7}$$

When n represents the number of pairs of distances separated by a length h, based on the fundamental equation for interpolation in Equation 4, and considering the analysis of variance for two positional data points, the interpolation equation using the kriging method can be expressed as shown in Equation 8.

$$Z(X_0) = \sum_{i=1}^{N} \lambda_i Z(x_i) + [1 - \sum_{i=1}^{N} \lambda_i]\mu \tag{8}$$

In this context, μ represents a known stationary mean. The parameter μ is considered constant throughout the entire domain and is determined as the average of the data. For ordinary kriging, Equation 8 will be applied under the condition that $[1 - \sum_{i=1}^{N} \lambda_i] = 0$ is specified, meaning that $\sum_{i=1}^{N} \lambda_i = 1$ is a straightforward property derived from this mathematical conditioning approach.

2.2.5. Support Vector Machine (SVM) Analysis

SVM is a machine learning tool classified as Supervised Learning, based on Statistical Learning Theory. It is used to classify data points by constructing a Hyperplane in an N-dimensional space, where N represents the number of features used to classify the data points, as illustrated in **Fig. 3**. In this research, SVM was used to classify Land Cover, which plays a significant role in studying the spatial interpolation of the LST variable.

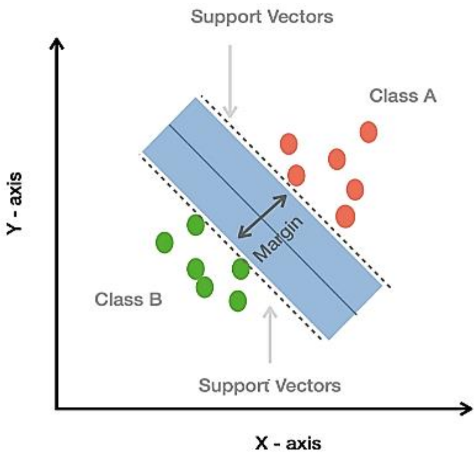

Fig. 3. Support Vector Machine (SVM) Analysis.

2.2.6. Statistical Testing

One of the most critical steps in model development is evaluating the accuracy of the model's predictions. Therefore, in this research, three statistical tests were employed: The first is Mean Absolute Error (MAE), a widely popular metric calculated by averaging the absolute errors, as shown in Equation 9 (Kostpoulou; 2021) . The second is Mean Squared Error (MSE), a method for measuring accuracy by addressing the problem of Mean Error (ME), which considers the squared differences between actual and predicted values, as shown in Equation 10 (Li et al, 2022). The third is Root Mean Squared Error (RMSE), which measures error by comparing the square root of the mean squared differences between predicted and actual values, as shown in Equation 11 (Zhou et al, 2019).

$$MAE = \frac{1}{n}\sum_{i=1}^{n}/y - y_i/ \quad (9)$$

$$\text{MSE} = \frac{1}{n}\sum_{i=1}^{n}(y - y_i)^2 \quad (10)$$

$$\text{RMSE} = \sqrt{\frac{1}{n}\sum_{i=1}^{n}(y - y_i)^2} \quad (11)$$

where:
y represents the actual measured data
y_i denotes the data derived from the model and
n signifies the total number of data points**.**

3. RESULTS

3.1. Land Use/Land Cover Analysis

The land area of Talat Sub-district, Maha Sarakham Province, Thailand, based on data from the Land Development Department, can be classified into four categories of Land Use/Land Cover: Agriculture, Marsh, Urban, and Water, as shown in **Fig. 4**. The figure is divided into two parts: 4 (a) and 4 (b), which depict the Land Use/Land Cover of Talat Sub-district in 2018 and 2023, respectively. For clarity and detail, the classification of Land Use/Land Cover in Talat Sub-district, Maha Sarakham Province, is presented in **Table 2**.

Table 2.

Land Use/Land Cover Classification

Class	Sub class	Description
Agriculture; A	A0	Integrated farm/Diversified farm
	A1	Abandoned paddy field
	A3	Abandoned perennial
	A4	Mango
	A5	Floricultural/Ornamental plant
	A7	Cattle farm house
	A8	Lotus
	A9	Abandoned aquaculture land
Marsh; M	M1	Shrubland
	M2	Marsh and Swamp
	M2+A1	Marsh and Swamp + Active paddy field
	M4	Landfill
Urban; U	U1	City, Town, Commercial
	U2	Village
	U3	Institutional land
	U4	Road
	U5	Factory
	U6	Resort, Hotel, Guesthouse
Water; W	W1	River, Canal
	W2	Farm pond

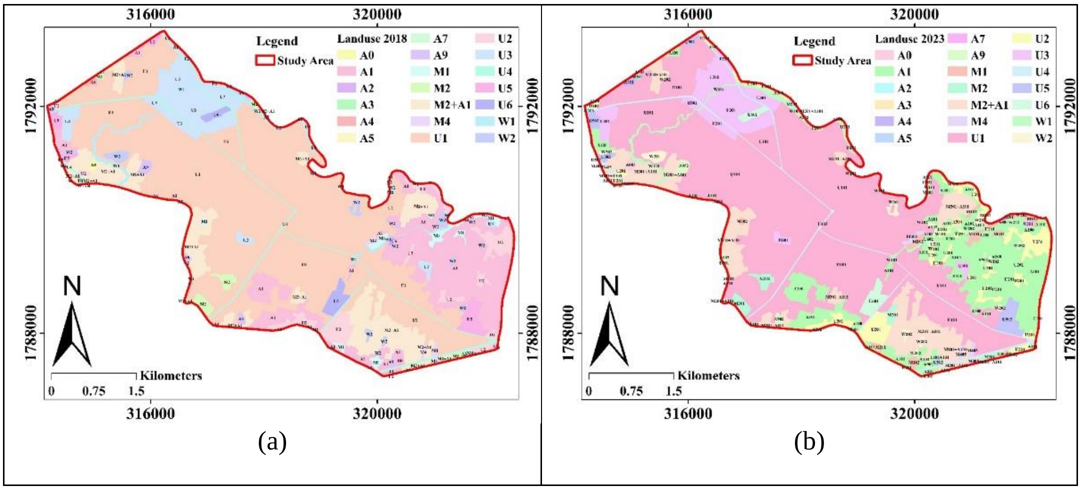

Fig. 4. Support Vector Machine (SVM) Analysis.

3.2. LST Analysis Using LANDSAT 8 Data

The results of LST analysis using LANDSAT 8 data are shown in **Fig. 5** (a) 2018 and (b) 2023), respectively. In 2018, the analysis revealed that the maximum, minimum, and average LST values were 30.553°C, 22.978°C, and 27.1608°C, respectively. In 2023, the analysis indicated maximum, minimum, and average LST values of 25.273°C, 18.280°C, and 21.534°C, respectively. The significant decrease in LST in 2023 compared to 2018 can be attributed to above-average rainfall in the study area during the rainy season from June to November 2022. This led to short-term flooding from late September to early October, resulting in increased soil moisture. Additionally, previously vacant areas experienced vegetation growth due to the increased rainfall, contributing to lower LST values. This observation aligns with ground temperature data from the Meteorological Department in Maha Sarakham Province, which recorded maximum, minimum, and average temperatures of 32.600°C, 20.220°C, and 26.400°C in December 2018, and 27.000°C, 18.000°C, and 22.000°C in December 2023, respectively.

Furthermore, the LST data calculated and generated from LANDSAT 8 satellite data for 2018 and 2023, when mapped as LST spatial data, revealed approximately 25,000 data points along the x and y planes.

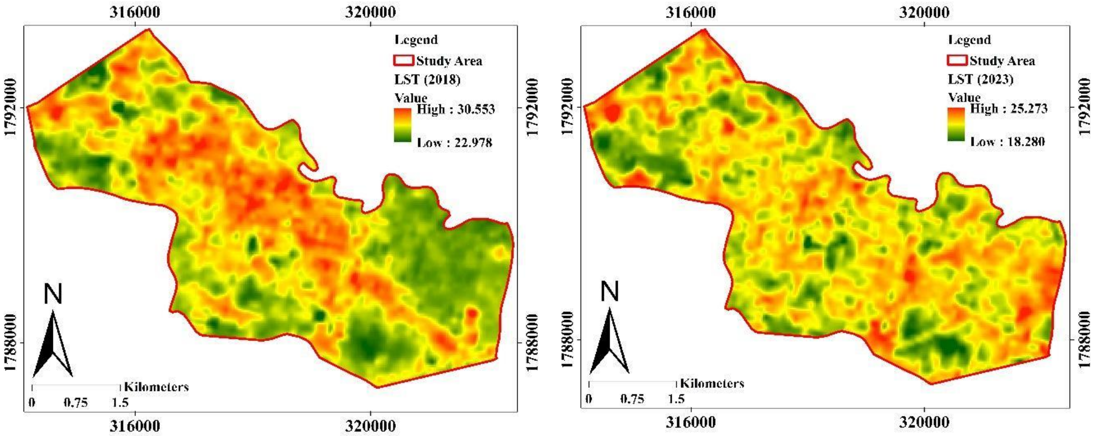

(a) (b)

Fig. 5. LST Analysis Using LANDSAT 8 Data.

This research extracted the data into two sets: the first set of 550 data points was used as initial parameters for interpolation techniques, including IDW, OK, and OK+SVM. After the interpolation process, each technique generated spatial data to create LST maps, resulting in the same number of data points as the LST maps calculated from LANDSAT 8 satellite data, totaling 25,000 data points. However, since 25,000 data points may be too numerous for evaluating and comparing the interpolated values from each technique, a second set of 1,650 data points, representing three times the initial data before interpolation, was extracted to serve as parameters for statistical testing to assess the model's consistency with direct LST calculations.

3.3. LST Analysis from Each Technique

The results of LST analysis from each technique in this study are shown in **Fig. 6** (a-d) and **7** (a-d). **Fig. 6** and **7** depict the LST analysis results for 2018 and 2023, respectively, with subfigures a-d for each year, (a) shows the LST analysis results, (b) shows the results using the IDW technique, (c) shows the results using the OK technique, and (d) shows the results using the OK+SVM technique. In **Fig. 6** (b) and **7** (b), which represent the traditional IDW interpolation technique, the maximum and minimum temperatures were 30.455°C and 23.939°C in 2018, and 23.991°C and 18.895°C in 2023, respectively. **Fig. 6** (c) and **7** (c) show the results of the OK technique, with maximum and minimum temperatures of 29.463°C and 24.868°C in 2018, and 22.725°C and 20.274°C in 2023, respectively. Finally, **Fig. 6** (d) and **7** (d) show the results of the OK+SVM technique, with maximum and minimum temperatures of 30.225°C and 24.388°C in 2018, and 23.311°C and 19.678°C in 2023, respectively.

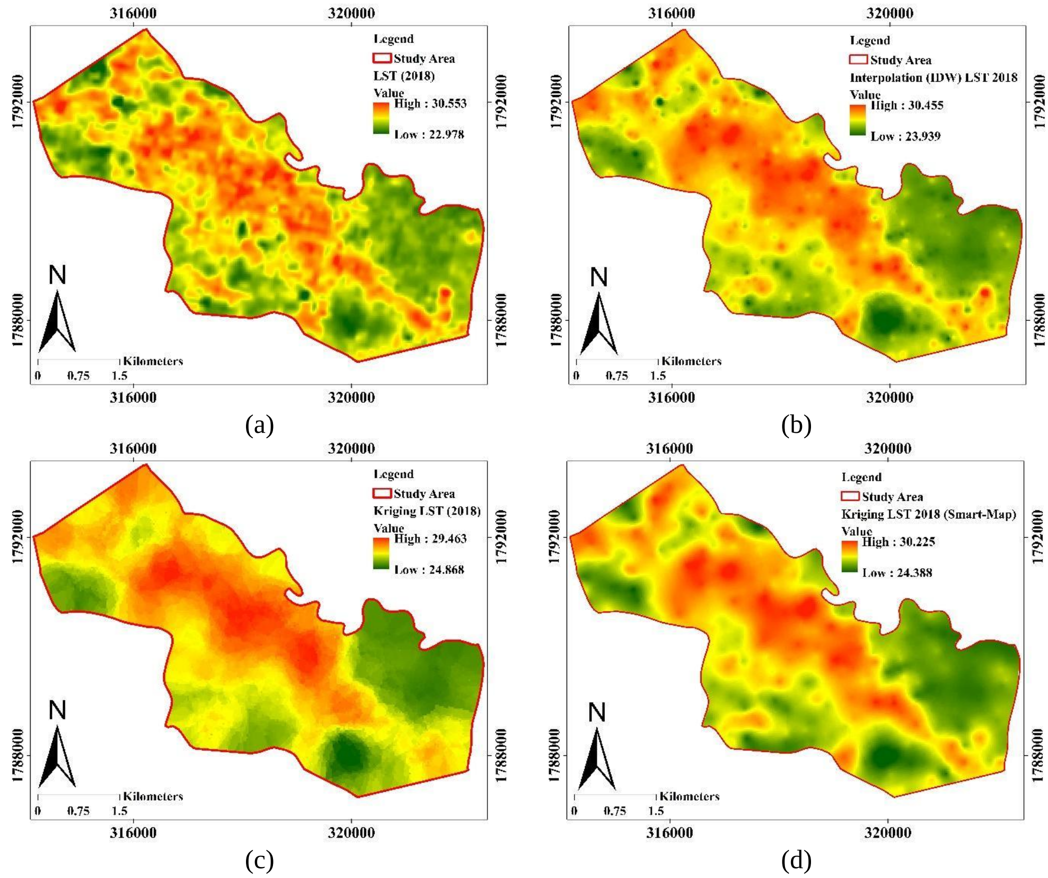

Fig. 6. LST Analysis in 2018 (a) LANDSAT 8, (b) IDW, (c) Ordinary kriging and (d) Ordinary kriging + SVM.

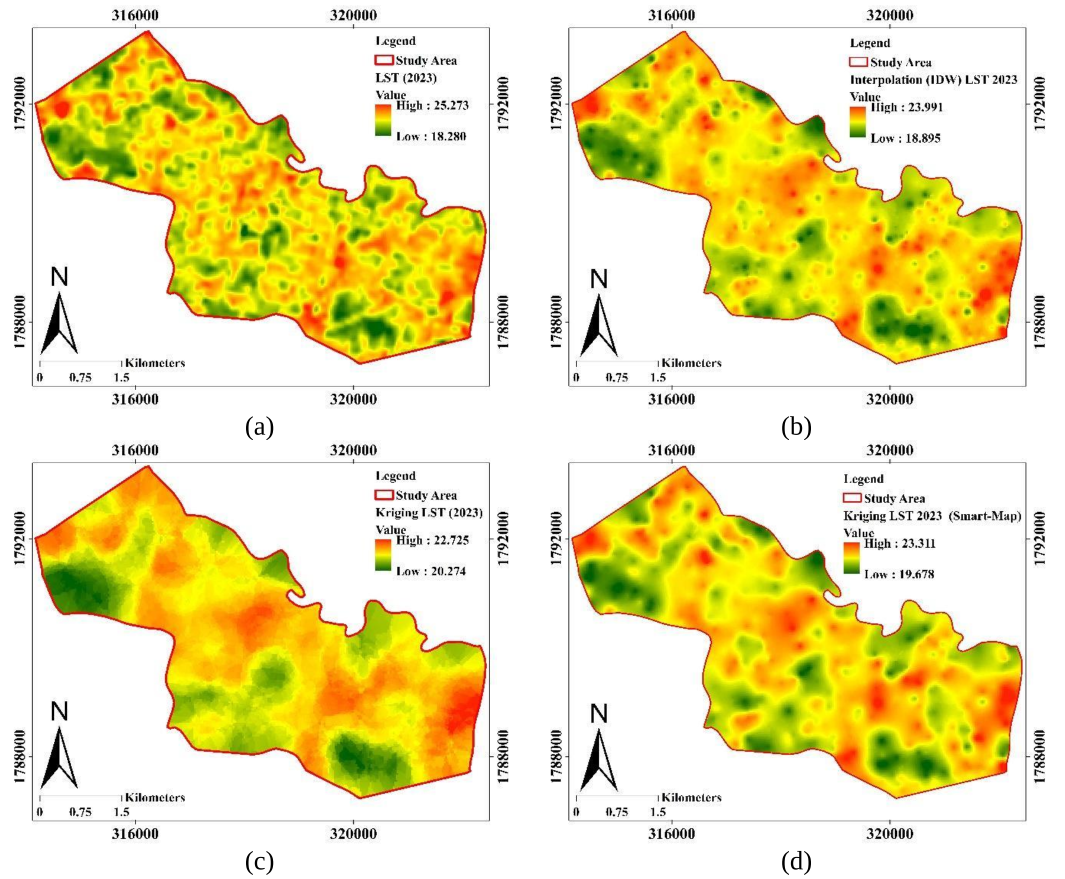

Fig. 7. LST Analysis in 2018 (a) LANDSAT 8, (b) IDW, (c) Ordinary kriging and (d) Ordinary kriging +SVM.

3.4. Maximum and Minimum Temperatures

The LST data, extracted in the form of maximum and minimum temperatures for each technique, is presented in **Table 3**. The differences between $\Delta T_{max} = \left| T_{LANDSAT8,max} - T_{Technique,max} \right|$ the maximum temperatures and $\Delta T_{min} = \left| T_{LANDSAT8,min} - T_{Technique,min} \right|$ the minimum temperatures were calculated and are also shown in **Table 3**. Maximum and minimum temperatures are the simplest and most straightforward variables for comparing the interpolation models of each technique.

The temperature differences were used as a criterion to evaluate the accuracy of the models, where $\Delta T_{min} \to 0$ and $\Delta T_{max} \to 0$ demonstrate that the interpolated temperatures closely match the actual measured temperatures. As shown in **Table 3**, in 2018, the values of ΔT_{max} and ΔT_{min} for the IDW technique were closest to 0, indicating that the interpolated maximum T_{max} and minimum T_{min} temperatures from this technique were the closest to the maximum and minimum temperatures calculated from LANDSAT 8 satellite data. The next closest techniques were OK+SVM and OK, respectively. In 2023, the trends for the differences in maximum ΔT_{max} and minimum

ΔT_{min} temperatures were similar to those in 2018, with the IDW technique producing values ΔT_{max} and ΔT_{min} closest to 0, followed by OK+SVM and OK, respectively.

However, while the maximum and minimum temperatures obtained from the interpolation of each technique are the simplest parameters for assessing the accuracy of each model, this variable is only a preliminary study and comparison of interpolated values. This is because values T_{max} and T_{min} represent data from a single point within the overall spatial variable under study. Nonetheless, the OK+SVM and OK techniques also produced values T_{max} and T_{min} that were close to the LANDSAT 8 values. One notable observation is that the OK+SVM technique provided T_{max} and T_{min} values closer to the LANSAT 8 temperatures, which suggests that the SVM learning method, combined with the OK interpolation incorporating the effects of LULC, led to more accurate interpolated temperatures that closely match the actual measured values.

Table 3.

Maximum and Minimum Temperatures.

Years	**Techniques**	T_{max}	T_{min}	ΔT_{max}	ΔT_{min}
2018	LANDSAT 8	30.553	22.978	-	-
	IDW	30.455	23.939	0.098	0.961
	OK	29.463	24.868	1.09	1.89
	OK+SVM	30.255	24.388	0.298	1.41
2023	LANDSAT 8	25.273	18.280	-	-
	IDW	23.991	18.895	1.282	0.615
	OK	22.725	20.274	2.548	1.994
	OK+SVM	23.311	19.678	1.962	1.398

3.5. Statistical Testing

To verify and compare the results obtained from the interpolation models of each technique, 1,650 spatial data points at the same (x,y) positions were extracted from the LST data of each technique to be compared with the data directly calculated from LANDSAT 8 satellite data. The statistical tests MAE, MSE, and RMSE, represented by Equations 9, 10, and 11, respectively, were used for evaluation. These three statistical measures were employed to assess and verify the models. A better statistical outcome is indicated when the values of these measures converge toward 0. The statistical test results for this study are presented in **Table 4**.

According to **Table 4**, in 2018, the MAE statistic for the OK+SVM technique yielded the lowest average error, which was 0.6682, followed by the IDW and OK techniques, respectively. Additionally, when the interpolation models were tested using the MSE and RMSE statistics, the OK+SVM technique also showed the smallest error dispersion, with values of 0.3827 and 0.6168, respectively, indicating less error dispersion compared to the IDW and OK techniques. In 2023, the MAE statistic for the OK+SVM technique again resulted in the lowest average error, which was 0.3609, followed by the IDW and OK techniques, respectively. The MSE and RMSE test statistics for the OK+SVM technique also showed the smallest error dispersion, with values of 0.2522 and 0.5022, respectively, indicating less error dispersion compared to the IDW and OK techniques. The results of comparing LST data obtained from each interpolation technique with the LST data analyzed using LANDSAT 8 satellite data indicate that the three statistical measures—MAE, MSE, and RMSE—demonstrate that the OK+SVM technique produced LST data closest to the LANDSAT 8 data.

Table 4.

Statistical Testing.

Years	Techniques	Static tests	Values
2018	IDW	MAE	0.4554
		MSE	0.4048
		RMSE	0.6362
	OK	MAE	0.6293
		MSE	0.6917
		RMSE	0.8317
	OK+SVM	MAE	0.4329
		MSE	0.3827
		RMSE	0.6186
2023	IDW	MAE	0.3838
		MSE	0.2788
		RMSE	0.5280
	OK	MAE	0.5201
		MSE	0.4465
		RMSE	0.6682
	OK+SVM	MAE	0.3609
		MSE	0.2522
		RMSE	0.5022

4. DISCUSSION

In the discussion of the operational results from the analysis of land use and LST analysis of Talat Sub-district, Mueang Maha Sarakham District, Maha Sarakham Province, Thailand, there are key aspects to consider in order to understand the results and their implications as follows: The classification of land use/land cover demonstrates significant changes in the area, particularly between 2018 and 2023, which may be attributed to both natural factors and human activities impacting land use, such as urban expansion and climate change.

The research conducted by Li et al., (Li et al, 2022). presents similar findings regarding land use changes in urban areas in China, highlighting the relationship between urban expansion and changes in the local environment. Concerning LST analysis, there was a clear shift in surface temperature values between 2018 and 2023, with the average temperature in 2023 being lower than in 2018. This might be due to higher than usual rainfall and the growth of vegetation in open spaces. Zhou et al. (Zhou et al, 2019), support this conclusion by indicating the impact of excessive rainfall on the reduction of surface temperature in suburban areas.

Regarding the analysis using various techniques such as IDW, OK, and OK+SVM, it was found that the OK+SVM technique provided the least error when compared to LANDSAT 8 satellite data, consistent with the research by Chen et al., (Chen, et al, 2020), which evaluated interpolation models and found that SVM techniques, when combined with other statistical methods, significantly improved prediction accuracy. Although the IDW technique provided the highest and lowest temperature values closest to actual data in some cases, in-depth analysis using OK+SVM still demonstrated higher accuracy in spatial estimation, possibly due to its ability to learn and adapt to more complex data characteristics.

From this discussion, it can be concluded that analyzing changes in land use and LST is crucial for understanding the impacts of climate change and land use on the local environment. The use of appropriate interpolation techniques can help obtain more accurate and reliable data, which will be beneficial for sustainable land resource planning and management in the future.

5. CONCLUSIONS

This research focuses on the improvement and comparison of traditional data inference techniques such as Inverse Distance Weighted (IDW) and Ordinary Kriging (OK), enhanced by the use of Support Vector Machines (SVM) to increase numerical accuracy. The OK + SVM method integrates the OK inference concept with SVM learning to classify land use types and assign weights to spatial data inference related to Land Surface Temperature (LST) in urban areas. The research findings indicate that the IDW technique yields Tmax and Tmin values closest to the actual measured values, followed by OK + SVM and OK, respectively. However, when assessing the inferred data from 1,650 points extracted from LST using each technique and testing with MAE, MSE, and RMSE statistics, it was found that OK + SVM provided better results than IDW and OK. In conclusion, OK + SVM offers superior inference outcomes compared to traditional inference techniques.

Data Availability Statement: data are available on request.

REFERENCES

Auntarin, C., Chunpang., P., Chokkuea, W., & Laosuwan, T. (2021). Using a Split-window Algorithm for the Retrieval of the Land Surface Temperature via Landsat-8 OLI/TIRS. *Geographia Technica*, 16(Special Issue), 70-81. https://doi.org/10.21163/GT_2021.163.03

Bennett, J.M., Sunday, J., Calosi, P., Villalobos, F., Martínez, B., Molina-Venegas, R., Araújo, M.B., Algar, A.C., Clusella-Trullas, S., Hawkins, B.A. & Keith, S.A., (2021) The evolution of critical thermal limits of life on Earth. *Nature communications*, 12(1), 1198. https://doi.org/10.1038/s41467-021-21263-8

Binarti, F., & Santoso, A. J. (2023). Identifying Climate Change Vulnerability Based On Land Cover Indicators: A Case Study in Surabaya, Indonesia. *Geographia Technica*, 18(1), 71–84. https://doi.org/10.21163/gt_ 2023.181.06

Cai, X., Wang, X., Jain, P., & Flannigan, M. D. (2019). Evaluation of gridded precipitation data and interpolation methods for forest fire danger rating in Alberta, Canada. *Journal of Geophysical Research: Atmospheres*, 124(1), 3-17. https://doi.org/10.1029/2018JD028754

Chen, Y., Nan, Z., Zhao, S., & Xu, Y. (2020). A Bayesian approach for interpolating clear-sky MODIS land surface temperatures on areas with extensive missing data. *IEEE Journal of Selected Topics in Applied Earth Observations and Remote Sensing*, 14, 515-528. https://doi.org/10.1109/JSTARS.2020.3038188

Cilek, M. U., & Cilek, A. (2021). Analyses of land surface temperature (LST) variability among local climate zones (LCZs) comparing Landsat-8 and ENVI-met model data. *Sustainable Cities and Society*, 69, 102877. https://doi.org/10.1016/j.scs.2021.102877

Cristóbal, J., Jiménez-Muñoz, J. C., Prakash, A., Mattar, C., Skoković, D., & Sobrino, J. A. (2018). An improved single-channel method to retrieve land surface temperature from the Landsat-8 thermal band. *Remote Sensing*, 10(3), 431. https://doi.org/10.3390/rs10030431

Dahlke, F. T., Wohlrab, S., Butzin, M., & Pörtner, H. O. (2020). Thermal bottlenecks in the life cycle define climate vulnerability of fish. *Science*, 369(6499), 65-70. https://doi.org/10.1126/science.aaz3658

Du, P., Bai, X., Tan, K., Xue, Z., Samat, A., Xia, J., Li, E., Su, H. and Liu, W., 2020. Advances of four machine learning methods for spatial data handling: A review. *Journal of Geovisualization and Spatial Analysis*, 4, pp.1-25. https://doi.org/10.1007/s41651-020-00048-5

Duan, S.B., Li, Z.L., Li, H., Göttsche, F.M., Wu, H., Zhao, W., Leng, P., Zhang, X. & Coll, C., (2019) Validation of Collection 6 MODIS land surface temperature product using in situ measurements. *Remote sensing of environment*, 225, 16-29. https://doi.org/10.1016/j.rse.2019.02.020

Fouedjio, F., & Klump, J. (2019). Exploring prediction uncertainty of spatial data in geostatistical and machine learning approaches. *Environmental Earth Sciences*, 78(1), 38. https://doi.org/10.1007/s12665-018-8032-z

Fuhg, J. N., Fau, A., & Nackenhorst, U. (2021). State-of-the-art and comparative review of adaptive sampling methods for kriging. *Archives of Computational Methods in Engineering*, 28, 2689-2747. https://doi.org/10.1007/s11831-020-09474-6

Fung, K. F., Chew, K. S., Huang, Y. F., Ahmed, A. N., Teo, F. Y., Ng, J. L., & Elshafie, A. (2022). Evaluation of spatial interpolation methods and spatiotemporal modeling of rainfall distribution in Peninsular Malaysia. *Ain Shams Engineering Journal*, 13(2), 101571. https://doi.org/10.1016/j.asej.2021.09.001

Gia Pham, T., Kappas, M., Van Huynh, C., & Hoang Khanh Nguyen, L. (2019). Application of ordinary kriging and regression kriging method for soil properties mapping in hilly region of Central Vietnam. *ISPRS International Journal of Geo-Information*, 8(3), 147. https://doi.org/10.3390/ijgi8030147

Giustini, F., Ciotoli, G., Rinaldini, A., Ruggiero, L., & Voltaggio, M. (2019). Mapping the geogenic radon potential and radon risk by using Empirical Bayesian Kriging regression: A case study from a volcanic area of central Italy. *Science of the Total Environment*, 661, 449-464. https://doi.org/10.1016/j.scitotenv.2019.01.146

Granville, K., Woolford, D. G., Dean, C. B., Boychuk, D., & McFayden, C. B. (2023). On the selection of an interpolation method with an application to the Fire Weather Index in Ontario, Canada. *Environmetrics*, 34(2), e2758. https://doi.org/10.1002/env.2758

Guha, S., Govil, H., & Diwan, P. (2020). Monitoring LST-NDVI Relationship Using Premonsoon Landsat Datasets. *Advances in Meteorology*, 2020(1), 4539684. https://doi.org/10.1155/2020/4539684

Guha, S., & Govil, H. (2021). An assessment on the relationship between land surface temperature and normalized difference vegetation index. *Environment, Development and Sustainability*, 23, 1944-1963. https://doi.org/10.1007/s10668-020-00657-6

Hu, Q., Li, Z., Wang, L., Huang, Y., Wang, Y., & Li, L. (2019). Rainfall spatial estimations: A review from spatial interpolation to multi-source data merging. *Water*, 11(3), 579. https://doi.org/10.3390/w11030579

Huang, M., Piao, S., Ciais, P., Peñuelas, J., Wang, X., Keenan, T.F., Peng, S., Berry, J.A., Wang, K., Mao, J. & Alkama, R., (2019). Air temperature optima of vegetation productivity across global biomes. *Nature ecology & evolution*, 3(5), 772-779. https://doi.org/10.1038/s41559-019-0838-x

Karakuş, C. B. (2019). The impact of land use/land cover (LULC) changes on land surface temperature in Sivas City Center and its surroundings and assessment of Urban Heat Island. *Asia-Pacific Journal of Atmospheric Sciences*, 55(4), 669-684. https://doi.org/10.1007/s13143-019-00109-w

Kartal, S., & Sekertekin, A. (2022). Prediction of MODIS land surface temperature using new hybrid models based on spatial interpolation techniques and deep learning models. *Environmental Science and Pollution Research*, 29(44), 67115-67134. https://doi.org/10.1007/s11356-022-20572-9

Khan, M., Almazah, M. M., EIlahi, A., Niaz, R., Al-Rezami, A. Y., & Zaman, B. (2023). Spatial interpolation of water quality index based on Ordinary kriging and Universal kriging. *Geomatics, Natural Hazards and Risk*, 14(1), 2190853. https://doi.org/10.1080/19475705.2023.2190853

Khosravi, Y., & Balyani, S. (2019). Spatial modeling of mean annual temperature in Iran: comparing cokriging and geographically weighted regression. *Environmental Modeling & Assessment*, 24, 341-354. https://doi.org/10.1007/s10666-018-9623-5

Kostopoulou, E. (2021). Applicability of ordinary Kriging modeling techniques for filling satellite data gaps in support of coastal management. *Modeling Earth Systems and Environment*, 7(2), 1145-1158.) https://doi.org/10.1007/s40808-020-00940-5

Kovács, K. D. & Haidu, I. (2022). Spatial effect of anti-COVID measures on land surface temperature (LST) in urban areas. *IDOJARAS*, 126(2), 203-232. https://doi.org/10.28974/idojaras.2022.2.3

Krivoruchko, K., & Gribov, A. (2019). Evaluation of empirical Bayesian kriging. *Spatial Statistics*, 32, 100368. https://doi.org/10.1016/j.spasta.2019.100368

Li, H., Peng, J., Yanxu, L., & Yi'na, H. (2017). Urbanization impact on landscape patterns in Beijing City, China: A spatial heterogeneity perspective. *Ecological Indicators*, 82, 50-60. https://doi.org/10.1016/j.ecolind.2017.06.032Get rights and content

Li, S., Griffith, D. A., & Shu, H. (2020). Temperature prediction based on a space–time regression-kriging model. *Journal of Applied Statistics*, 47(7), 1168-1190. https://doi.org/10.1080/02664763.2019.1671962

Li, Y., Baorong, Z., Xiaohong, X., & Zijun, L. (2022). Application of a semivariogram based on a deep neural network to Ordinary Kriging interpolation of elevation data. *Plos one*, 17(4), e0266942. https://doi.org/10.1371/journal.pone.0266942 A

Li, Z. (2021). An enhanced dual IDW method for high-quality geospatial interpolation. *Scientific reports*, 11(1), 9903. https://doi.org/10.1038/s41598-021-89172-w

Li, Z.L., Wu, H., Duan, S.B., Zhao, W., Ren, H., Liu, X., Leng, P., Tang, R., Ye, X., Zhu, J. & Sun, Y., (2023) Satellite remote sensing of global land surface temperature: Definition, methods, products, and applications. *Reviews of Geophysics*, 61(1). https://doi.org/10.1029/2022RG000777

Magyari-Sáska, Z., Haidu, I., & Magyari-Sáska, A. (2025). Experimental Comparative Study on Self-Imputation Methods and Their Quality Assessment for Monthly River Flow Data with Gaps: Case Study to Mures River. *Applied Sciences*, 15(3), 1242. https://doi.org/10.3390/app15031242

Militino, A. F., Ugarte, M. D., Pérez-Goya, U., & Genton, M. G. (2019). Interpolation of the mean anomalies for cloud filling in land surface temperature and normalized difference vegetation index. *IEEE Transactions on Geoscience and Remote Sensing*, *57*(8), 6068-6078. https://doi.org/10.1109/TGRS.2019.2904193

Moustapha, M., Bourinet, J. M., Guillaume, B., & Sudret, B. (2018). Comparative study of Kriging and support vector regression for structural engineering applications. *ASCE-ASME Journal of Risk and Uncertainty in Engineering Systems, Part A: Civil Engineering*, 4(2), 04018005. https://doi.org/10.1061/AJRUA6.0000950

Munyati, C., & Sinthumule, N. I. (2021). Comparative suitability of ordinary kriging and Inverse Distance Weighted interpolation for indicating intactness gradients on threatened savannah woodland and forest stands. *Environmental and Sustainability Indicators*, 12, 100151. https://doi.org/10.1016/j.indic.2021.100151

Nord, A., & Giroud, S. (2020). Lifelong effects of thermal challenges during development in birds and mammals. *Frontiers in Physiology*, 11, 419. https://doi.org/10.3389/fphys.2020.00419

Palafox-Juárez, E.B., López-Martínez, J.O., Hernández-Stefanoni, J.L. & Hernández-Nuñez, H., (2021) Impact of urban land-cover changes on the spatial-temporal land surface temperature in a tropical City of Mexico. *ISPRS International Journal of Geo-Information*, 10(2), 76. https://doi.org/10.3390/ijgi10020076

Pede, T., & Mountrakis, G. (2018). An empirical comparison of interpolation methods for MODIS 8-day land surface temperature composites across the conterminous Unites States. *ISPRS journal of photogrammetry and remote sensing*, *142*, 137-150. https://doi.org/10.1016/j.isprsjprs.2018.06.003

Phan, T. N., & Kappas, M. (2018). Application of MODIS land surface temperature data: a systematic literature review and analysis. *Journal of Applied Remote Sensing*, 12(4), 041501-041501. https://doi.org/10.1117/1.JRS.12.041501

Prohmdirek, T., Chunpang, P., & Laosuwan, T. (2020). The Relationship between Normalized Difference Vegetation Index and Canopy Temperature that affects the urban heat island phenomenon. *Geographia Technica*, 15(2), 222–234. https://doi.org/10.21163/gt_2020.152.21

Rashid, N., Alam, J. M., Chowdhury, M. A., & Islam, S. L. U. (2022). Impact of landuse change and urbanization on urban heat island effect in Narayanganj city, Bangladesh: A remote sensing-based estimation. *Environmental Challenges*, 8, 100571. https://doi.org/10.1016/j.envc.2022.100571

Rosillon, D. J., Jago, A., Huart, J. P., Bogaert, P., Journée, M., Dandrifosse, S., & Planchon, V. (2024). Near real-time spatial interpolation of hourly air temperature and humidity for agricultural decision support systems. *Computers and Electronics in Agriculture*, 223, 109093. https://doi.org/10.1016/j.compag.2024.109093

Sangüesa, C., Pizarro, R., Ingram, B., Ibáñez, A., Rivera, D., García-Chevesich, P., Pino, J., Pérez, F., Balocchi, F. and Peña, F., (2023) Comparing Methods for the Regionalization of Intensity− Duration− Frequency (IDF) Curve Parameters in Sparsely-Gauged and Ungauged Areas of Central Chile. *Hydrology*, 10(9), 179. https://doi.org/10.3390/hydrology10090179

Sekulić, A., Kilibarda, M., Heuvelink, G. B., Nikolić, M., & Bajat, B. (2020). Random forest spatial interpolation. *Remote Sensing*, 12(10), 1687. https://doi.org/10.3390/rs12101687

Shahfahad, Kumari, B., Tayyab, M., Ahmed, I. A., Baig, M. R. I., Khan, M. F., & Rahman, A. (2020). Longitudinal study of land surface temperature (LST) using mono-and split-window algorithms and its relationship with NDVI and NDBI over selected metro cities of India. *Arabian Journal of Geosciences*, 13, 1-19. https://doi.org/10.1007/s12517-020-06068-1

Shtiliyanova, A., Bellocchi, G., Borras, D., Eza, U., Martin, R., & Carrère, P. (2017). Kriging-based approach to predict missing air temperature data. *Computers and Electronics in Agriculture*, 142, 440-449. https://doi.org/10.1016/j.compag.2017.09.033

Singh, P., Sarkar Chaudhuri, A., Verma, P., Singh, V. K., & Meena, S. R. (2022). Earth observation data sets in monitoring of urbanization and urban heat island of Delhi, India. *Geomatics, Natural Hazards and Risk*, 13(1), 1762-1779. https://doi.org/10.1080/19475705.2022.2097452

Singh, P., & Verma, P. (2019). A comparative study of spatial interpolation technique (IDW and Kriging) for determining groundwater quality. *GIS and geostatistical techniques for groundwater science*, 43-56. https://doi.org/10.1016/B978-0-12-815413-7.00005-5

Subedi, M. R., Xi, W., Edgar, C. B., Rideout-Hanzak, S., & Hedquist, B. C. (2019). Assessment of geostatistical methods for spatiotemporal analysis of drought patterns in East Texas, USA. *Spatial Information Research*, 27, 11-21. https://doi.org/10.1007/s41324-018-0216-9

Thompson, N. A., Higham, J. P., Heistermann, M., Vogel, E., & Cords, M. (2020). Energy balance but not competitive environment corresponds with allostatic load during development in an Old World monkey. *Hormones and Behavior*, 119, 104664. https://doi.org/10.1016/j.yhbeh.2019.104664

Vedantu. Interpolation. Available online: https://www.vedantu.com/maths/interpolation (accessed on 25 September 2024).

Venter, Z. S., Brousse, O., Esau, I., & Meier, F. (2020). Hyperlocal mapping of urban air temperature using remote sensing and crowdsourced weather data. *Remote Sensing of Environment*, 242, 111791. https://doi.org/10.1016/j.rse.2020.111791

Xiao, H., Kopecká, M., Guo, S., Guan, Y., Cai, D., Zhang, C., Zhang, X. and Yao, W., 2018. Responses of urban land surface temperature on land cover: A comparative study of Vienna and Madrid. *Sustainability*, 10(2), 260. https://doi.org/10.3390/su10020260

Yang, W., Zhao, Y., Wang, D., Wu, H., Lin, A., & He, L. (2020). Using principal components analysis and IDW interpolation to determine spatial and temporal changes of surface water quality of Xin'anjiang river in Huangshan, China. *International journal of environmental research and public health*, 17(8), 2942. https://doi.org/10.3390/ijerph17082942

Zhang, Z., & Du, Q. (2019). A bayesian kriging regression method to estimate air temperature using remote sensing data. *Remote Sensing*, 11(7), 767. https://doi.org/10.3390/rs11070767

Zhou, L., Meng, Y., & Abbaspour, K. C. (2019). A new framework for multi-site stochastic rainfall generator based on empirical orthogonal function analysis and Hilbert-Huang transform. *Journal of Hydrology*, 575, 730-742. https://doi.org/10.1016/j.jhydrol.2019.05.047